Eur. Phys. J. E **31**, 159–167 (2010)
DOI 10.1140/epje/i2010-10558-6

THE EUROPEAN PHYSICAL JOURNAL E

Regular Article

Leak rate of seals: Effective-medium theory and comparison with experiment

B. Lorenz and B.N.J. Persson[a]

IFF, FZ Jülich, D-52425 Jülich, Germany

Received 16 November 2009
Published online: 1 March 2010 – © EDP Sciences / Società Italiana di Fisica / Springer-Verlag 2010

Abstract. Seals are extremely useful devices to prevent fluid leakage. We present an effective-medium theory of the leak rate of rubber seals, which is based on a recently developed contact mechanics theory. We compare the theory with experimental results for seals consisting of silicon rubber in contact with sandpaper and sand-blasted PMMA surfaces.

1 Introduction

A seal is a device for closing a gap or making a joint fluid tight [1]. Seals play a crucial role in many modern engineering devices, and the failure of seals may result in catastrophic events, such as the Challenger disaster. In spite of its apparent simplicity, it is not easy to predict the leak rate and (for dynamic seals) the friction forces [2]. The main problem is the influence of surface roughness on the contact mechanics at the seal-substrate interface. Most surfaces of engineering interest have surface roughness on a wide range of length scales [3], *e.g.*, from cm to nm, which will influence the leak rate and friction of seals, and accounting for the whole range of surface roughness is impossible using standard numerical methods, such as the Finite Element Method.

We have recently presented experimental results for the leak rate of rubber seals [4], and compared the results to a "critical-junction" theory [3,5,6], which is based on percolation theory and a recently developed contact mechanics theory [7–14]. Here we will report on new experimental data, and compare the experimental results with the critical-junction theory, and also to an extension of this theory presented below, which is based on the effective-medium approach.

2 Critical-junction theory

We first briefly review the leak rate model developed in refs. [3,5,6]. Consider the fluid leakage through a rubber seal, from a high fluid pressure P_a region, to a low fluid pressure P_b region, as in fig. 1. Assume that the nominal contact region between the rubber and the hard countersurface is rectangular with area $L_x \times L_y$, with $L_y > L_x$.

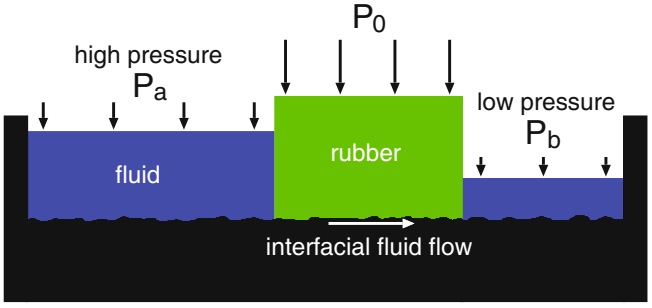

Fig. 1. Rubber seal (schematic). The liquid on the left-hand side is under the hydrostatic pressure P_a and the liquid to the right under the pressure P_b (usually, P_b is the atmospheric pressure). The pressure difference $\Delta P = P_a - P_b$ results in liquid flow at the interface between the rubber seal and the rough substrate surface. The volume of liquid flow per unit time is denoted by $\dot{Q}$, and depends on the squeezing pressure P_0 acting on the rubber seal.

We assume that the high pressure fluid region is for $x < 0$ and the low pressure region for $x > L_x$. We "divide" the contact region into squares with side $L_x = L$ and area $A_0 = L^2$ (this assumes that $N = L_y/L_x$ is an integer, but this restriction does not affect the final result). Now, let us study the contact between the two solids within one of the squares, as we change the magnification ζ. We define $\zeta = L/\lambda$, where λ is the resolution. We study how the apparent contact area (projected on the xy-plane), $A(\zeta)$, between the two solids depends on the magnification ζ. At the lowest magnification we cannot observe any surface roughness, and the contact between the solids appears to be complete *i.e.*, $A(1) = A_0$. As we increase the magnification we will observe some interfacial roughness, and the (apparent) contact area will decrease. At high enough magnification, say $\zeta = \zeta_c$, a percolating path of

[a] e-mail: b.persson@fz-juelich.de

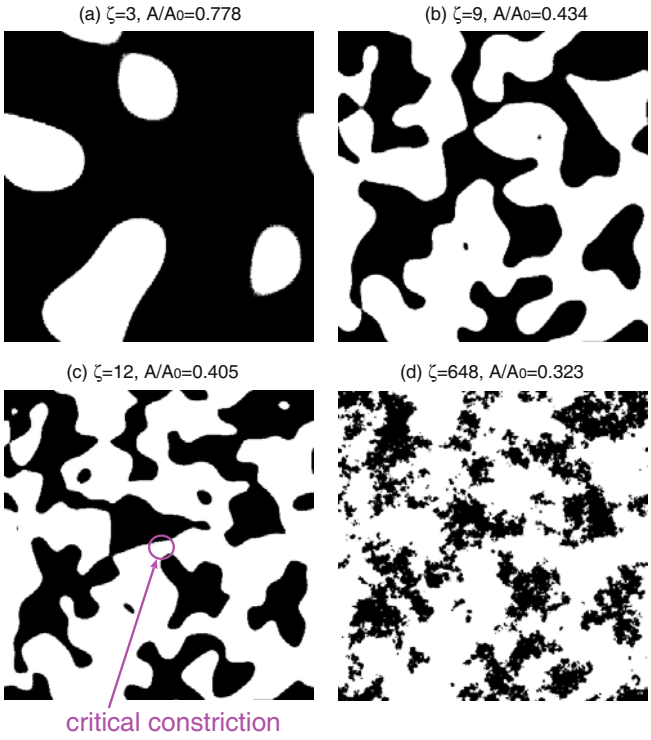

Fig. 2. The contact region at different magnifications $\zeta = 3$, 9, 12 and 648, is shown in (a)–(d), respectively. When the magnification increases from 9 to 12 the non-contact region percolates. At the lowest magnification $\zeta = 1$: $A(1) = A_0$. The figure is the result of Molecular Dynamics simulations of the contact between elastic solids with randomly rough surfaces, see ref. [6].

non-contact area will be observed for the first time, see fig. 2. We denote the most narrow constriction along this percolation path as the *critical constriction*. The critical constriction will have the lateral size $\lambda_c = L/\zeta_c$ and the surface separation at this point is denoted by u_c. We can calculate u_c using a recently developed contact mechanics theory [12] (see below). As we continue to increase the magnification we will find more percolating channels between the surfaces, but these will have more narrow constrictions than the first channel which appears at $\zeta = \zeta_c$, and as a first approximation one may neglect the contribution to the leak rate from these channels [6].

A first rough estimate of the leak rate is obtained by assuming that all the leakage occurs through the critical percolation channel, and that the whole pressure drop $\Delta P = P_a - P_b$ (where P_a and P_b is the pressure to the left and right of the seal) occurs over the critical constriction (of width and length $\lambda_c \approx L/\zeta_c$ and height u_c). We will refer to this theory as the "critical-junction" theory. If we approximate the critical constriction as a pore with rectangular cross-section (width and length λ_c and height $u_c \ll \lambda_c$), and if we assume an incompressible Newtonian fluid, the volume flow per unit time through the critical constriction will be given by (Poiseuille flow)

$$\dot{Q} = \frac{u_c^3}{12\eta}\Delta P, \tag{1}$$

where η is the fluid viscosity. In deriving (1) we have assumed laminar flow and that $u_c \ll \lambda_c$, which is always satisfied in practice. We have also assumed no-slip boundary condition on the solid walls. This assumption is not always satisfied at the micro- or nano-scale, but is likely to be a very good approximation in the present case owing to surface roughness which occurs at length scales shorter than the size of the critical constriction. Finally, since there are $N = L_y/L_x$ square areas in the rubber-countersurface (apparent) contact area, we get the total leak rate

$$\dot{Q} = \frac{L_y}{L_x}\frac{u_c^3}{12\eta}\Delta P. \tag{2}$$

Note that a given percolation channel could have several narrow (critical or nearly critical) constrictions of nearly the same dimension which would reduce the flow along the channel. But in this case one would also expect more channels from the high to the low fluid pressure side of the junction, which would tend to increase the leak rate. These two effects will, at least in the simplest picture where one assumes that the distance between the critical junctions along a percolation path (in the x-direction) is the same as the distance between the percolation channels (in the y-direction), compensate each other (see ref. [6]). The effective-medium theory presented below includes (in an approximate way) all the flow channels.

To complete the theory, we must calculate the separation u_c of the surfaces at the critical constriction. We first determine the critical magnification ζ_c by assuming that the apparent relative contact area at this point is given by percolation theory. Thus, the relative contact area $A(\zeta)/A_0 \approx 1-p_c$, where p_c is the so-called percolation threshold [20]. For infinite-sized 2D systems, and assuming site percolation $p_c \approx 0.70$ for a hexagonal lattice, 0.59 for a square lattice, and 0.5 for a triangular lattice [20]. For bond percolation the corresponding numbers are 0.65, 0.5, and 0.35, respectively. For continuous percolation in 2D the Bruggeman effective-medium theory predicts $p_c = 0.5$, and since we want to compare the critical-junction theory to the prediction of the effective-medium theory we will use $p_c = 0.5$ in the critical-junction theory. For finite-sized systems the percolation will, on the average, occur for (slightly) smaller values of p_c, and fluctuations in the percolation threshold will occur between different realizations of the same physical system. In earlier studies we have used $p_c = 0.6$ to determine the critical magnification $\zeta = \zeta_c$. However, the new experimental data presented below agree better with the critical-junction theory when $p_c \approx 0.5$. Numerical simulations such as those presented in ref. [6] (see fig. 2) and ref. [21] typically give p_c slightly larger than 0.5.

The (apparent) relative contact area $A(\zeta)/A_0$ at the magnification ζ can be obtained using the contact mechanics formalism developed elsewhere [7,9–12], where the system is studied at different magnifications ζ. We have [7,8]

$$\frac{A(\zeta)}{A_0} = \frac{1}{(\pi G)^{1/2}}\int_0^{P_0} \mathrm{d}\sigma\, \mathrm{e}^{-\sigma^2/4G} = \mathrm{erf}\left(\frac{P_0}{2G^{1/2}}\right),$$

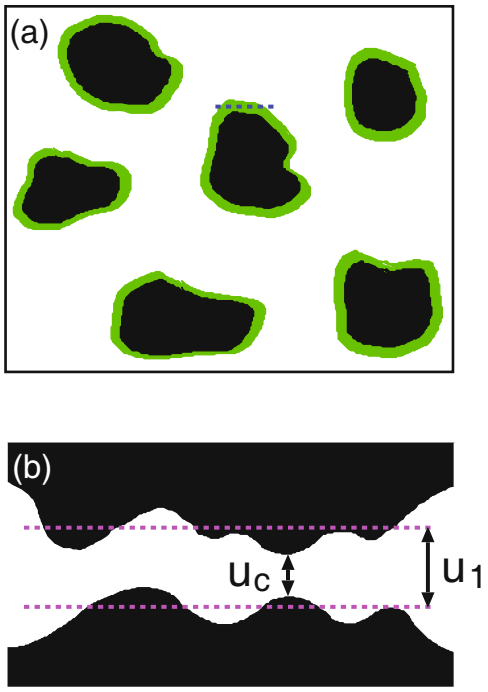

Fig. 3. (Colour on-line) (a) The black area represents the asperity contact regions at magnification ζ. The green area is the additional contact area observed when the magnification is reduced to $\zeta - \Delta\zeta$ (where $\Delta\zeta$ is small). The average separation between the solid walls in the green surface area is denoted by $u_1(\zeta)$. (b) Separation between the solid walls along the blue dashed line in (a). Since the surfaces of the solids are everywhere rough, the actual separation between the solid walls in the green area will fluctuate around the average $u_1(\zeta)$. At the most narrow constriction the surface separation is u_c.

where

$$G(\zeta) = \frac{\pi}{4}\left(\frac{E}{1-\nu^2}\right)^2 \int_{q_0}^{\zeta q_0} \mathrm{d}q q^3 C(q),$$

where the surface roughness power spectrum

$$C(q) = \frac{1}{(2\pi)^2}\int \mathrm{d}^2x \langle h(\mathbf{x})h(\mathbf{0})\rangle \mathrm{e}^{-i\mathbf{q}\cdot\mathbf{x}},$$

where $\langle \ldots \rangle$ stands for ensemble average. Here E and ν are Young's elastic modulus and the Poisson ratio of the rubber. The height profile $h(\mathbf{x})$ of the rough surface can be measured routinely today on all relevant length scales using optical and stylus experiments.

We define $u_1(\zeta)$ to be the (average) height separating the surfaces which appear to come into contact when the magnification decreases from ζ to $\zeta - \Delta\zeta$, where $\Delta\zeta$ is a small (infinitesimal) change in the magnification. In fig. 3(a) the black area represents the asperity contact regions at magnification ζ. The green area is the additional contact area observed when the magnification is reduced to $\zeta - \Delta\zeta$ (where $\Delta\zeta$ is small) [22]. The average separation between the solid walls in the green surface area is given by $u_1(\zeta)$. Figure 3(b) shows the separation between the solid walls along the dashed line in fig. 3(a). Since the surfaces of the solids are everywhere rough, the actual separation between the solid walls in the green area will fluctuate around the average $u_1(\zeta)$. Thus we expect $u_c = \alpha u_1(\zeta_c)$, where $\alpha < 1$ (but of order unity, see fig. 3(b)) [23]. We note that α is due to the surface roughness which occurs at length scales shorter than λ_c, and it may be possible to calculate (or estimate) α from the surface roughness power spectrum, but no such theory has been developed so far and here we treat α as a fit parameter.

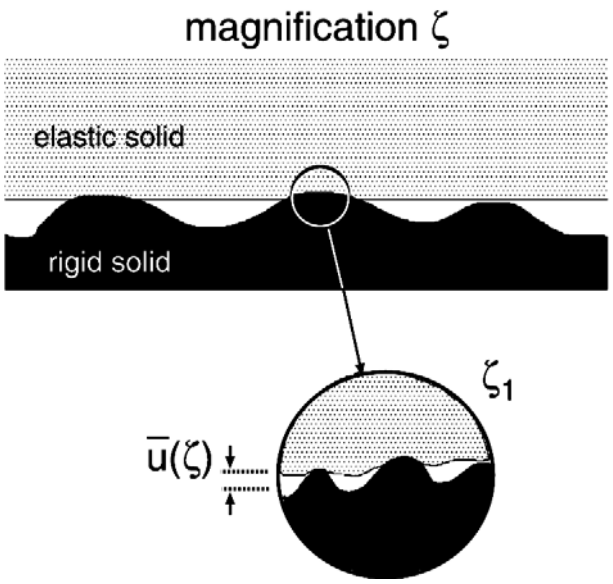

Fig. 4. An asperity contact region observed at magnification ζ. It appears that complete contact occurs in the asperity contact region, but when the magnification is increasing to the highest (atomic scale) magnification ζ_1, it is observed that the solids are actually separated by the average distance $\bar{u}(\zeta)$.

$u_1(\zeta)$ is a monotonically decreasing function of ζ, and can be calculated from the average interfacial separation $\bar{u}(\zeta)$ and $A(\zeta)$ using (see ref. [12])

$$u_1(\zeta) = \bar{u}(\zeta) + \bar{u}'(\zeta)A(\zeta)/A'(\zeta).$$

The quantity $\bar{u}(\zeta)$ is the average separation between the surfaces in the apparent contact regions observed at magnification ζ, see fig. 4. It can be calculated from [12]

$$\bar{u}(\zeta) = \sqrt{\pi}\int_{\zeta q_0}^{q_1} \mathrm{d}q\, q^2 C(q) w(q,\zeta) \int_{p(\zeta)}^{\infty} \mathrm{d}p' \frac{1}{p'} e^{-[w(q,\zeta)p'/E^*]^2},$$

where $p(\zeta) = p_0 A_0/A(\zeta)$ and

$$w(q,\zeta) = \left(\pi \int_{\zeta q_0}^{q} \mathrm{d}q'\, q'^3 C(q')\right)^{-1/2}.$$

One can show from the equations above that as the applied squeezing pressure $p_0 \to 0$, for the magnifications most relevant for calculating the leak rate of seals, $u_1 \to \bar{u}$.

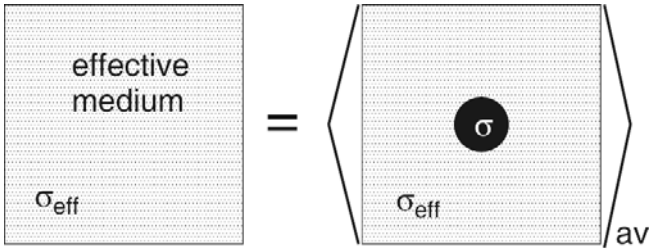

Fig. 5. Effective-medium theories take into account random disorder in a physical system, *e.g.*, random fluctuations in the interfacial separation $u(\mathbf{x})$. Thus, for a n-component system (*e.g.*, where the separation u takes n different discrete values) one assumes that the flow in the effective medium should be the same as the average fluid flow obtained when circular regions of the n-components are embedded in the effective medium. Thus, for example, the pressure p at the origin calculated assuming that the effective medium occurs everywhere must equal the average $\sum c_i p_i$ (where c_i is the concentration of component i) of the pressures p_i (at the origin) calculated with the circular inclusion of component $i = 1, \ldots, n$.

3 Effective-medium theory

The critical-junction theory presented above assumes that the leak rate is determined by the resistance towards fluid flow through the critical constriction (or through a network of critical constrictions, see above). In reality there will be many flow channels at the interface. Here we will use the 2D Bruggeman effective-medium theory to calculate (approximately) the leak rate resulting from the network of flow channels.

Using the 2D Bruggeman effective-medium theory, we get (see ref. [24], fig. 5, and appendix A):

$$\dot{Q} = \frac{L_y}{L_x}\sigma_{\rm eff}\Delta P, \tag{3}$$

where $\Delta P = P_{\rm a} - P_{\rm b}$ is the pressure drop and where (see appendix A)

$$\frac{1}{\sigma_{\rm eff}} = \int {\rm d}\sigma\, P(\sigma)\frac{2}{\sigma_{\rm eff}+\sigma} = \int {\rm d}\zeta \left(-\frac{A'(\zeta)}{A_0}\right)\frac{2}{\sigma_{\rm eff}+\sigma(\zeta)}, \tag{4}$$

where

$$\sigma(\zeta) = \frac{[\alpha u_1(\zeta)]^3}{12\eta}. \tag{5}$$

Equation (4) is easy to solve by iteration.

It is not clear that the effective-medium theory is better than the critical-junction theory. One problem with this theory is the following: In the effective-medium model there is no correlation between the size of a region and the (average) separation between the surfaces in the region. In reality, the regions where the surface separation is large form large compact (or connected) regions (since they are observed already at low magnification).

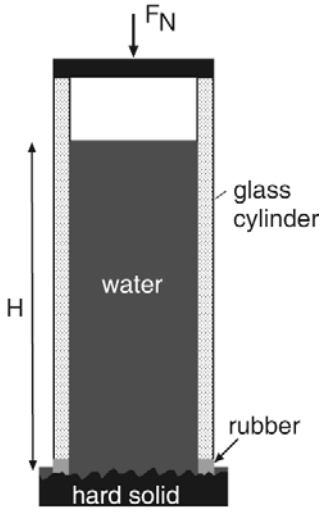

Fig. 6. Experimental set-up for measuring the leak rate of seals. A glass (or PMMA) cylinder with a rubber ring attached to one end is squeezed against a hard substrate with well-defined surface roughness. The cylinder is filled with water, and the leak rate of the water at the rubber-countersurface is detected by the change in the height of the water in the cylinder.

4 Experimental

We have performed a very simple experiment to test the theory presented above. In fig. 6 we show our set-up for measuring the leak rate of seals. A glass (or PMMA) cylinder with a rubber ring (with rectangular cross-section) attached to one end is squeezed against a hard substrate with well-defined surface roughness. The cylinder is filled with water, and the leak rate of the fluid at the rubber-countersurface is detected by the change in the height of the fluid in the cylinder. In this case the pressure difference $\Delta P = P_{\rm a} - P_{\rm b} = \rho g H$, where g is the gravitation constant, ρ the fluid density and H the height of the fluid column. With $H \approx 1\,{\rm m}$ we get typically $\Delta P \approx 0.01\,{\rm MPa}$. With the diameter of the glass cylinder of order a few cm, the condition $P_0 \gg \Delta P$ (which is necessary in order to be able to neglect the influence on the contact mechanics from the fluid pressure at the rubber-countersurface) is satisfied already for loads (at the upper surface of the cylinder) of order kg. In our study we use a rubber ring with Young's elastic modulus $E = 2.3\,{\rm MPa}$, and with the inner and outer diameter 3 cm and 4 cm, respectively, and height 0.5 cm. The rubber ring was made from a silicon elastomer (PDMS) prepared using a two-component kit (Sylgard 184) purchased from Dow Corning (Midland, MI). The kit consists of a base (vinyl-terminated polydimethylsiloxane) and a curing agent (methylhydrosiloxane-dimethylsiloxane copolymer) with a suitable catalyst. From these two components we prepared a mixture 10:1 (base/cross-linker) in weight. The mixture was degassed to remove the trapped air induced by stirring from the mixing process and then poured into casts. The bottom of these casts was made from glass

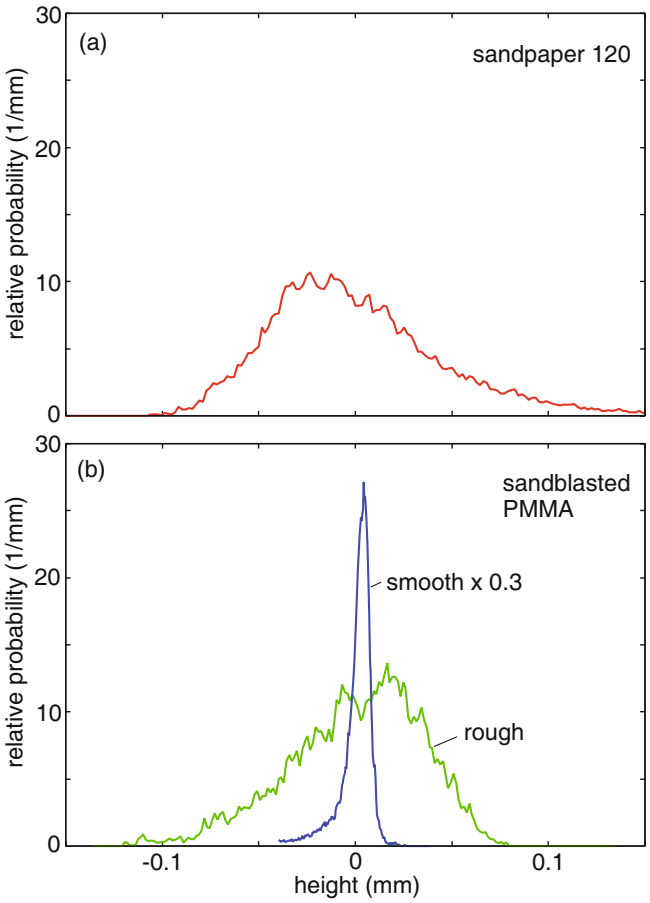

Fig. 7. The surface height probability distribution of (a) sandpaper 120, and (b) two sand-blasted PMMA. The surfaces have root-mean-square roughness of 44 μm, 34 μm, and 10 μm, respectively, and the surface area (including only the surface roughness with wave vector indicated in the figure) is about 49%, 28% and 10% larger, respectively, than the nominal surface area A_0 (*i.e.*, the surface area projected on the xy-plane).

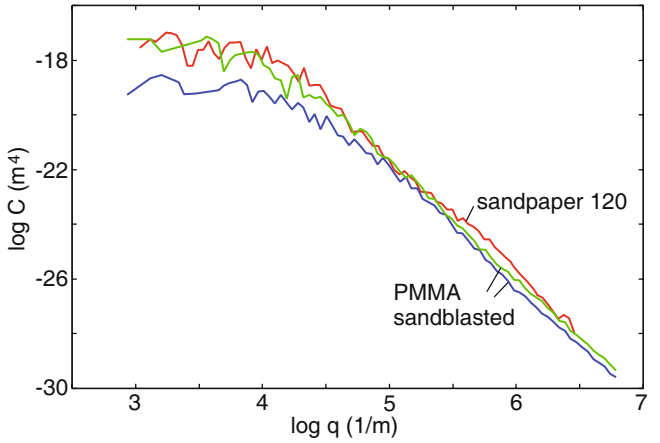

Fig. 8. Surface roughness power spectrum of sandpaper 120 and two sand-blasted PMMA. The surfaces have root-mean-square roughness of 44 μm, 34 μm, and 10 μm, respectively, and the surface area (including only the surface roughness with wave vector indicated in the figure) is about 49%, 28% and 10% larger, respectively, than the nominal surface area A_0 (*i.e.*, the surface area projected on the xy-plane).

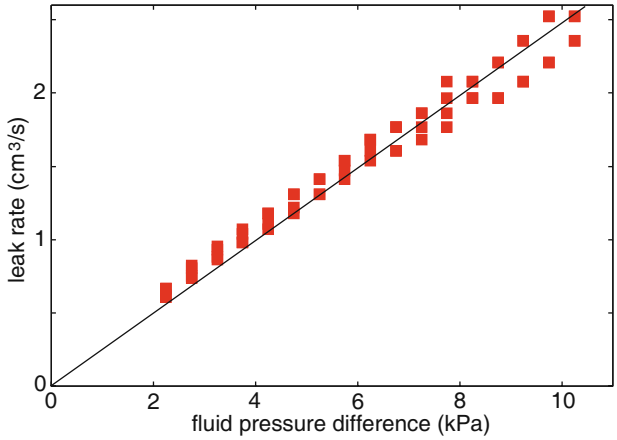

Fig. 9. Square symbols: the measured leak rate for different fluid pressure drop $\Delta P = P_a - P_b$ for the nominal squeezing pressure $P_0 \approx 60$ kPa. For the sandpaper surface.

to obtain smooth surfaces. The samples were cured in an oven at 80 °C for 12 h.

We have used sandpaper and sand-blasted PMMA as substrates. The sandpaper (corundum paper, grit size 120) has a root-mean-square roughness of 44 μm. From the measured surface topography we obtain the height probability distribution $P(h)$ and the surface roughness power spectrum $C(q)$ shown in fig. 7(a) and fig. 8, respectively. Sand paper has much sharper and larger roughness than the counter surfaces used in normal rubber seal applications. However, from a theory point of view it should not really matter on which length scale the roughness occurs, except for "complications" such as the influence of adhesion and fluid contamination particles (which tend to clog the flow channels). Nevertheless, the theory assumes that the average surface slope is not too large, and we have therefore also measured the leak rate for rubber seal in contact with sand-blasted Plexiglas with less sharp roughness.

Our first experiment with a relative smooth Plexiglas (PMMA) surface showed that the leak rate decreased by time and finally no leaking could be observed. But this experiment used unfiltered tap water containing contamination particles which clogged the channels. Using distilled water we found the leak rate (for a given fluid pressure difference) to be practically time independent. In fig. 7(b) and fig. 8 we show the height probability distribution $P(h)$ and the power spectrum $C(q)$ of the two sand-blasted PMMA used below. The root-mean-square roughness of the two surfaces is 34 μm and 10 μm.

5 Experimental results and analysis

According to (1) and (3), we expect the leak rate to increase linearly with the fluid pressure difference $\Delta P = P_a - P_b$. We first performed some experiments to test this prediction. In fig. 9 we show the measured leak rate (for

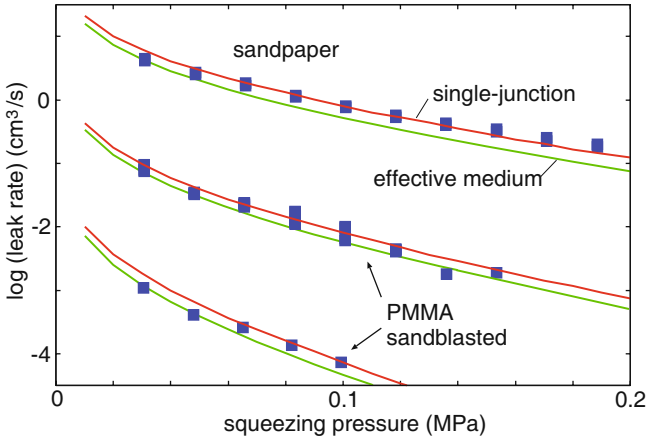

Fig. 10. (Colour on-line) Square symbols: the measured leak rate for ten different squeezing pressures for sandpaper 120 (upper data points) and sand-blasted PMMA (lower two sets of data points). In each case the green lines are the calculated leak rate using the effective-medium theory and the red lines using the critical-junction theory. In the calculation we used the measured surface topography, the measured rubber elastic modulus $E = 2.3\,\mathrm{MPa}$ and the fluid pressure difference $\Delta P = P_\mathrm{a} - P_\mathrm{b} = 10\,\mathrm{kPa}$ obtained from the height of the water column. In the calculations we have used $\alpha = 0.73$ (for sandpaper) and 0.31 (for PMMA).

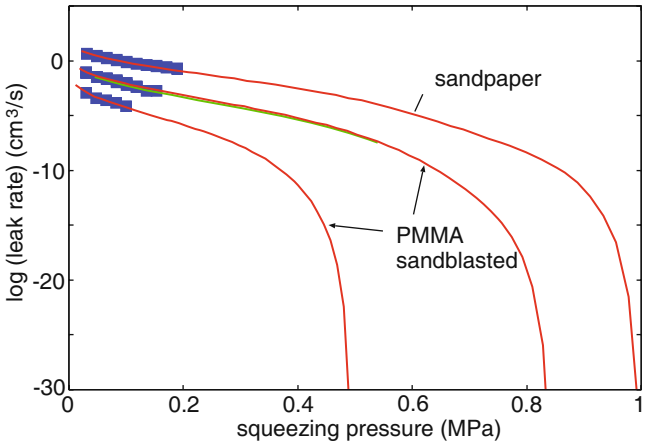

Fig. 11. (Colour on-line) Same as in fig. 10 but for a larger range of squeezing pressures. The red lines are the results of the critical-junction theory. The effective-medium theory gives practically the same results, as illustrated for the rough sand-blasted PMMA (green curve).

the sandpaper surface) for different fluid pressure drop ΔP for the nominal squeezing pressure $P_0 \approx 60\,\mathrm{kPa}$. To within the accuracy of the experiment, the leak rate depends linearly on ΔP.

In fig. 10 we show the logarithmic (with 10 as basis) of the measured leak rate for several different squeezing pressures (square symbols). We show results for both the sandpaper surface and for the two sand-blasted PMMA surfaces. The solid lines are the calculated leak rate using the measured rubber elastic modulus $E = 2.3\,\mathrm{MPa}$ and the surface power spectrum $C(q)$ shown in fig. 8. We show calculations using both the critical-junction theory (red lines) and the effective-medium theory (green lines). In the calculations we have used $\alpha = 0.73$ (for sandpaper) and 0.31 (for PMMA). Note that the two theories give remarkable similar results.

In fig. 11 we show the same as in fig. 10 but for a larger range of squeezing pressures. The red lines are the results of the critical-junction theory. The effective-medium theory gives practically the same results, as illustrated for the rough sand-blasted PMMA (green curve). Note that for the sandpaper, and the rough and smooth PMMA, for squeezing pressures above 1.0, 0.85 and 0.49 MPa, respectively, no percolating non-contact flow channels occur at the interface, and the leak rate vanishes.

6 Discussion

We have presented experimental results for the leak rate for a PDMS rubber ring (with rectangular cross-section), squeezed against three different surfaces: two sand-blasted PMMA surfaces and a sandpaper 120 surface. The experimental results have been compared to a simple critical-junction theory and to a (more accurate) effective-medium theory. The basic input in both theories is information about the interfacial surface separation, which we have obtained using the contact mechanics theory of Persson. The pressure dependence predicted by both theories is in very good agreement with the experimental data.

The contact mechanics theory we use assumes randomly rough surfaces. Randomly rough surfaces have a Gaussian height probability distribution $P(h)$. However, most surfaces of engineering interest have not Gaussian height probability distribution. In fig. 7 we show the height distribution for the surfaces used in the present study. Note that $P(h)$ is asymmetric with a tail towards higher h for the sandpaper surface, and towards smaller (negative) h for the sand-blasted PMMA surfaces. This is easy to understand: the sandpaper surfaces consist of particles with sharp edges pointing above the surface, while the region between particles are filled with a resin-binder making the valleys smoother and wider than the peaks, which result in an asymmetric $P(h)$ as observed. The PMMA surfaces are prepared by bombarding a flat PMMA surface with small hard particles. This results, at least for a short time of sand-blasting, in local indentations (where the particles hit the surface) separated by smoother surface regions, leading to the observed asymmetry in the height distribution.

Let us now discuss how the asymmetry in the height distribution may effect the leak rate. To illustrate this we consider an extreme case: a rigid solid block with a flat surface in contact with a rigid substrate with periodic "roughness" as in fig. 12. The substrate surfaces in (a) and (b) have the same surface roughness power spectrum, but it is clear that in (a) the empty volume between the surfaces is larger than in (b), resulting in a larger leak rate. In the real situation the roughness is not periodic and the solids are not rigid, but one may expect a higher

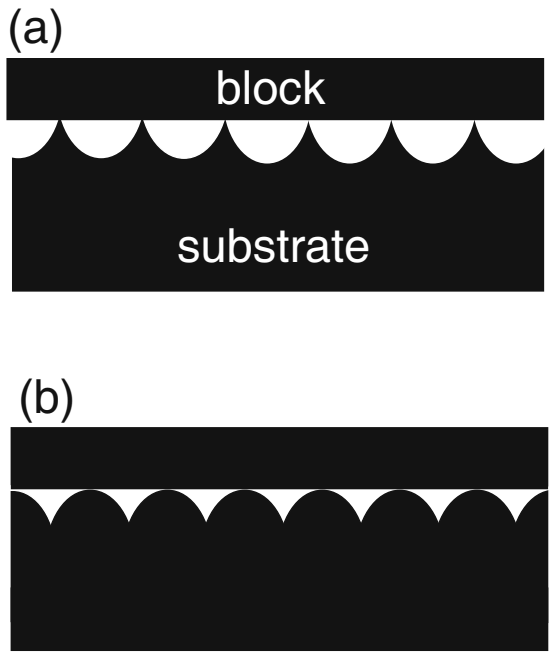

Fig. 12. Contact between a rigid block with a flat surface and a rigid substrate with periodic surface structures. The two substrate surfaces in (a) and (b) have the same surface roughness power spectrum. Note that the empty volume between the surfaces is much larger in the case (a) than in case (b).

leak rate for the situation where the asymmetry of the height profile is the same as for the sandpaper surface. We suggest that this may be the physical origin of why the factor α is larger for the sandpaper surface as compared to the PMMA surfaces. Another observation which supports this conclusion is the fact that the surface roughness power spectrum of the rough PMMA surface and the sandpaper 120 surface are very similar, but the leak rate differs by roughly two orders of magnitude. This indicates that some aspects of the surface topography, not contained in the power spectrum, are likely to be important. We note that for randomly rough surfaces, the statistical properties of the surfaces are fully contained in the power spectrum $C(q)$, *i.e.*, for this case only $C(q)$ will enter in the theory for the leak rate.

To study the point discussed above, we plan to perform an experiment where we "invert" the roughness of the sandpaper surface by producing a "negative" of the original surface using silicon rubber. In this experiment we will squeeze a silicon rubber ring, which is cross-linked with the sandpaper surface as the substrate, against a flat glass surface. By comparing the measured leak rate for this configuration with that for a silicon ring with flat bottom surface squeezed against the same sandpaper surface, we will be able to address the problem illustrated in fig. 12.

As an alternative to using the effective-medium approach to calculate the leak rate of seals, one may use the so-called critical-path analysis [25–27]. This approach has recently been applied to seals [28] but in contrast to the effective-medium theory, there enter two parameters which are not easy to obtain from theory. Since the effective-medium approach has been found to be rather accurate (see, *e.g.*, ref. [29]), we believe this approach to be more suitable for calculating the leak rate of seals.

7 Summary and conclusion

To summarize, we have compared experimental data with theory for the leak rate of seals. The theory is based on percolation theory and a recently developed contact mechanics theory. The experiments are for silicon rubber seals in contact with sandpaper and two sand-blasted PMMA surfaces. The elastic properties of the rubber and the surface topography of the sandpaper and PMMA surfaces are fully characterized. The dependence of the calculated leak rate $\dot{Q}$ on the squeezing pressure is in good agreement with experiment. The simplest version of the theory only accounts for fluid flow through the percolation channels observed at (or close to) the percolation threshold. We have also presented another approach based on the effective-medium approximation. This theory also includes flow channels observed at higher magnification, but gives leak rates remarkably similar to the critical-junction theory.

We thank G. Carbone for useful comments on the manuscript. This work, as part of the European Science Foundation EUROCORES Program FANAS, was supported from funds by the DFG and the EC Sixth Framework Program, under contract N ERAS-CT-2003-980409.

Appendix A.

Here we briefly review the effective-medium approach for calculating the fluid flow through an interface where the separation $u(\mathbf{x})$ between the surfaces varies with the lateral coordinate $\mathbf{x} = (x, y)$. If $u(\mathbf{x})$ varies slowly with $\mathbf{x}$, the Navier-Stokes equation of fluid flow reduces to

$$\mathbf{J} = -\sigma \nabla p, \tag{A.1}$$

where the conductivity $\sigma = u^3(\mathbf{x})/12\eta$.

In the effective-medium approach one replaces the local, spatial varying, conductivity $\sigma(\mathbf{x})$ with a constant effective conductivity $\sigma_{\rm eff}$. Thus the fluid flow current equation,

$$\mathbf{J} = -\sigma_{\rm eff} \nabla p, \tag{A.2}$$

as applied to a rectangular region $L_x \times L_y$ with the 2D pressure gradient $\mathrm{d}p/\mathrm{d}x = (P_{\rm b} - P_{\rm a})/L_x$, gives

$$\dot{Q} = L_y J_x = \frac{L_y}{L_x} \sigma_{\rm eff} \Delta P, \tag{A.3}$$

where $\Delta P = P_{\rm a} - P_{\rm b}$ is the pressure drop.

The effective-medium conductivity $\sigma_{\rm eff}$ is obtained as follows. Let us study the current flow at a circular inclusion (radius R) with the (constant) conductivity σ located

in an infinite conducting sheet with (constant) conductivity $\sigma_{\rm eff}$. We introduce polar coordinates with the origin at the center of the circular inclusion. The current

$$\mathbf{J} = -\sigma\nabla p, \quad \text{for} \quad r < R,$$
$$\mathbf{J} = -\sigma_{\rm eff}\nabla p, \quad \text{for} \quad r > R.$$

We consider a steady state so that

$$\nabla \cdot \mathbf{J} = 0,$$

or

$$\nabla^2 p = 0. \tag{A.4}$$

If $\mathbf{J}_0 = -\sigma_{\rm eff}\mathbf{a}$ is the current far from the inclusion (assumed to be constant) we get, for $r > R$,

$$p = [1 + f(r)]\mathbf{a} \cdot \mathbf{x}. \tag{A.5}$$

Equation (A.4) is satisfied if

$$f''(r) + 3f'(r)r^{-1} = 0.$$

A solution to this equation is $f = \alpha r^{-2}$. Substituting this in (A.5) gives

$$p = [1 + \alpha r^{-2}]\mathbf{a} \cdot \mathbf{x}. \tag{A.6}$$

For $r < R$ we have the solution

$$p = \beta\mathbf{a} \cdot \mathbf{x}. \tag{A.7}$$

Since p and $\mathbf{x} \cdot \mathbf{J}$ must be continuous at $r = R$, we get from (A.6) and (A.7)

$$1 + \alpha R^{-2} = \beta,$$
$$(1 - \alpha R^{-2})\sigma_{\rm eff} = \beta\sigma,$$

Combining these two equations gives

$$\beta = \frac{2\sigma_{\rm eff}}{\sigma_{\rm eff} + \sigma}\,. \tag{A.8}$$

The basic picture behind effective-medium theories is presented in fig. 5. Thus, for a two-component system, one assumes that the flow in the effective medium should be the same as the average fluid flow obtained when circular regions of the two components are embedded in the effective medium. Thus, for example, the pressure p calculated assuming that the effective medium occurs everywhere must equal the average $c_1p_1 + c_2p_2$ of the pressures p_1 and p_2 calculated with the circular inclusion of the two components **1** and **2**, respectively. For $r < R$ we have for the effective medium $p = \mathbf{a}\cdot\mathbf{x}$ and using (A.7) the equation $p = c_1p_1 + c_2p_2$ gives

$$1 = c_1\beta_1 + c_2\beta_2, \tag{A.9}$$

where c_1 and c_2 are the fractions of the total area occupied by the components **1** and **2**, respectively. Using (A.8) and (A.9) gives

$$1 = c_1\frac{2\sigma_{\rm eff}}{\sigma_{\rm eff} + \sigma_1} + c_2\frac{2\sigma_{\rm eff}}{\sigma_{\rm eff} + \sigma_2}\,,$$

which is the standard Bruggeman effective medium for a two-component system. Note that if one component is insulating, say $\sigma_2 = 0$, as $c_1 \to 0.5$ from above, $\sigma_{\rm eff} \to 0$, *i.e.*, $p_c = 1/2$ is the percolation threshold of the two-component 2D-Bruggeman effective-medium model.

If one instead has a continuous distribution of components (which we number by the continuous index ξ) with conductivities $\sigma = \sigma(\xi)$, then

$$1 = \int {\rm d}\xi\, P(\xi)\beta(\xi), \tag{A.10}$$

where $P(\xi)$ is the fraction of the total surface area occupied by the component denoted by ξ. The probability distribution $P(\xi)$ is normalized so that

$$\int {\rm d}\xi\, P(\xi) = 1. \tag{A.11}$$

Using (A.8) we get

$$1 = \int {\rm d}\xi\, P(\xi)\frac{2\sigma_{\rm eff}}{\sigma_{\rm eff} + \sigma(\xi)}\,. \tag{A.12}$$

It is easy to show from this equation that also for the case of a continuous distribution of components, the percolation limit occurs when the non-conducting component (which in our case corresponds to the area of real contact where $u = 0$ and hence $\sigma = u^3/12\eta = 0$) occupies 50% of the total surface area, *i.e.*, $p_c = 1/2$ in this case too.

References

1. R. Flitney, *Seals and Sealing Handbook* (Elsevier, 2007).
2. M. Mofidi, B. Prakash, B.N.J. Persson, O. Albohr, J. Phys.: Condens. Matter **20**, 085223 (2008).
3. See, *e.g.*, B.N.J. Persson, O. Albohr, U. Tartaglino, A.I. Volokitin, E. Tosatti, J. Phys.: Condens. Matter **17**, R1 (2005).
4. B. Lorenz, B.N.J. Persson, EPL **86**, 44006 (2009).
5. B.N.J. Persson, O. Albohr, C. Creton, V. Peveri, J. Chem. Phys. **120**, 8779 (2004).
6. B.N.J. Persson, C. Yang, J. Phys.: Condens. Matter **20**, 315011 (2008).
7. B.N.J. Persson, J. Chem. Phys. **115**, 3840 (2001).
8. B.N.J. Persson, Phys. Rev. Lett. **99**, 125502 (2007).
9. B.N.J. Persson, Surf. Sci. Rep. **61**, 201 (2006).
10. B.N.J. Persson, Eur. Phys. J. E **8**, 385 (2002).
11. B.N.J. Persson, F. Bucher, B. Chiaia, Phys. Rev. B **65**, 184106 (2002).
12. C. Yang, B.N.J. Persson, J. Phys.: Condens. Matter **20**, 215214 (2008).
13. B.N.J. Persson, J. Phys.: Condens. Matter **20**, 312001 (2008).
14. The contact mechanics model developed in refs. [7–13] takes into account the elastic coupling between the contact regions in the nominal rubber-substrate contact area. Asperity contact models, such as the "standard" contact mechanics model of Greenwood-Williamson [15], and the model of Bush *et al.* [16], neglect this elastic coupling, which results in highly incorrect results [17,18], in particular for the relations between the squeezing pressure and the interfacial separation [19].

15. J.A. Greenwood, J.B.P. Williamson, Proc. R. Soc. London, Ser. A **295**, 300 (1966).
16. A.W. Bush, R.D. Gibson, T.R. Thomas, Wear **35**, 87 (1975).
17. C. Campana, M.H. Müser, M.O. Robbins, J. Phys.: Condens. Matter **20**, 354013 (2008).
18. G. Carbone, F. Bottiglione, J. Mech. Phys. Solids **56**, 2555 (2008).
19. B. Lorenz, B.N.J. Persson, J. Phys.: Condens. Matter **201**, 015003 (2009).
20. D. Stauffer, A. Aharony, *An Introduction to Percolation Theory* (CRC Press, 1991).
21. See paper F in: F. Sahlin, *Lubrication, contact mechanics and leakage between rough surfaces*, PhD thesis (2008).
22. Figure 3(a) is schematic as in reality the contact islands at high enough magnification are fractal-like, and decreasing the magnification results in more complex changes than just adding strips (of constant width) of contact area to the periphery of the contact islands. However, this does not change our conclusions.
23. In ref. [12] the probability distribution of interfacial separations $\langle\delta(u-u(\mathbf{x}))\rangle$ as obtained from Molecular Dynamics calculations for self-affine fractal surfaces (with the fractal dimension $D_{\rm f} = 2.2$) was compared to the distribution of separations obtained from $u_1(\zeta)$. The former distribution was found to be about a factor of two wider than that obtained from $u_1(\zeta)$. This is consistent with the fact that $u_1(\zeta)$ is already an averaged separation and indicate that in this case $\alpha \approx 0.5$.
24. D. Bruggeman, Ann. Phys. Leipzig **24**, 636 (1935).
25. V.N. Ambegaokar, B.I. Halperin, J.S. Langer, Phys. Rev. B **4**, 2612 (1971).
26. A.G. Hunt, *Percolation Theory for Flow in Porous Media* (Springer, New York, 2005).
27. Z. Wu, E. Lopez, S.V. Buldyrev, L.A. Braunstein, S. Havlin, H.E. Stanley, Phys. Rev. E **71**, 045101(R) (2005).
28. F. Bottiglione, G. Carbone, L. Mangialardi, G. Mantriota, J. Appl. Phys. **106**, 104902 (2009).
29. S. Kirkpatrick, Rev. Mod. Phys. **45**, 574 (1973).